ASCE

Performance-Based Wind Engineering of Tall Buildings Examining Life-Cycle Downtime and Multisource Wind Damage

Wei Cui[1] and Luca Caracoglia, M.ASCE[2]

Abstract: Structural performance against wind hazards is necessary in modern tall building design. In current wind engineering practice, most efforts focus on structural safety, such as the avoidance of large deformations. Besides structural safety, other wind-induced inconveniences, such as downtime caused by loss of operability after a major wind event, have rarely been investigated. Furthermore, discomfort to occupants is often caused by less intense but more frequent winds. Consequently, the current wind load and design approach, predominantly based on extreme wind events, is not sufficient. This paper proposes a simulation framework for life-cycle downtime analysis of tall buildings. The approach combines three typical wind-induced inconveniences: occupants' discomfort, failure of key equipment, and nonstructural damages on the facade, which can lead to whole or partial loss of building functionality and, in turn, downtime. They are classified into two categories: frequent wind hazard inducing disturbance and extreme wind hazards causing damage. In the latter, both parent wind speed distribution and extreme wind distribution are found from data analysis, enabling evaluation of hazard occurrence probability. This study culminates with the estimation of a tall building's life-cycle downtime through year-by-year downtime accumulation. The result will be used to determine an optimal building orientation because wind directionality effect is not negligible in a typical local climate. **DOI: 10.1061/(ASCE)ST.1943-541X.0002479.**

Author keywords: Tall buildings; Wind-induced vibration; Occupants' comfort; Loss of functionality; Downtime.

Introduction

Skyscrapers are city landmarks and a center of human and social activities (e.g., Taipei 101, Burj Khalifa, and Shanghai World Financial Center). They greatly impact local culture, economy, and society; therefore, accurate evaluation of building performance under wind hazards is necessary. In recent years, the designation of performance-based design (PBD) has been emerging as an innovative tool to replace the traditional prescriptive design method (PDB). PDB was originally developed in seismic engineering and is based on the correspondence between earthquake recurrence intervals and performance levels (SEAOC 1995). The basic concept of PBD is to ensure that a structure satisfies a set of predefined performance requirements (Inokuma 2002) when subjected to various hazard levels. In the wind engineering field, implementation of similar PBD-inspired methods has been recently considered, as documented by recent studies examining this approach for various structures prone to wind-induced vibration (Ciampoli et al. 2011). Increasing intensity of hurricanes has also inspired research on the inelastic analysis of tall buildings under possibly destructive wind hazards during their life cycle (Huang et al. 2015).

In comparison with earthquakes, wind hazard has a much shorter recurrence interval scale, and moderate and mild wind hazards are more frequent. The definition of "performance" in wind engineering is different from that used in seismic engineering; it is known as performance-based wind engineering (PBWE). PBWE was first studied for low-rise buildings (van de Lindt and Dao 2009; Ellingwood et al. 2004) because structural collapse initiated by damage is a concept directly inspired by seismic engineering. In recent years, occupant discomfort has become a major concern for tall building design; several researchers (Bernardini et al. 2012, 2013; Kwok et al. 2009) have developed performance evaluation methods and optimization algorithms, emphasizing occupant comfort (Spence and Gioffrè 2012; Spence and Kareem 2014). Recently, building life-cycle intervention cost has been used as a structural performance indicator. This variable can integrate several damage types during a building's lifetime; it enables cost-effective design at an early stage by minimizing the maintenance planning in the aftermath of a catastrophic wind event (Cui and Caracoglia 2015, 2018b). Besides high- and low-rise buildings, PBWE has also been applied to long-span bridges (Seo and Caracoglia 2012, 2013).

The research group from Northeastern University examined several issues related to PBWE for vibration-sensitive structures, such as long-span bridges (Seo and Caracoglia 2012, 2013), pedestrian bridges (Rizzo et al. 2018), and tall buildings (Cui and Caracoglia 2015, 2016). Principal emphasis was given to the simulation and analysis of life-cycle intervention costs after a catastrophic wind event. The research was inspired by similar studies on monetary loss and structural performance analysis in seismic engineering (Wen and Kang 2001). Studies have lately been expanded through collaboration with the University of Perugia, Italy (Ierimonti et al. 2016, 2017). More recently, the

[1]Assistant Professor, State Key Lab of Disaster Reduction in Civil Engineering, Tongji Univ., Shanghai 200092, China; Key Laboratory of Transport Industry of Wind Resistant Technology for Bridge Structures, Tongji Univ., Shanghai 200092, China; Dept. of Bridge Engineering, College of Civil Engineering, Tongji Univ., Shanghai 200092, China. ORCID: https://orcid.org/0000-0001-7489-923X. Email: cuiwei@tongji.edu.cn

[2]Associate Professor, Dept. of Civil and Environmental Engineering, Northeastern Univ., 400 Snell Engineering Center, 360 Huntington Ave., Boston, MA 02115 (corresponding author). ORCID: https://orcid.org/0000-0002-4783-2600. Email: lucac@coe.neu.edu

Note. This manuscript was submitted on December 25, 2018; approved on May 22, 2019; published online on October 31, 2019. Discussion period open until March 31, 2020; separate discussions must be submitted for individual papers. This paper is part of the ***Journal of Structural Engineering***, © ASCE, ISSN 0733-9445.

PBWE theory for vertical structures affected by nonstationary thunderstorm downburst wind loads has been formulated (Le and Caracoglia 2018).

Despite these advancements, little emphasis has been given to moderate and mild wind events, despite them being much more frequent. Moderate and mild wind hazards may interrupt building's electric and mechanical systems, although nearly all structural elements are unaffected by damage. Because current tall buildings and skyscrapers are architecturally complex, integrating several different functionalities and losses originating from failures to electric or mechanical components may either partially or fully interrupt building's operations. This aspect is especially important because of the increasing number of smart civil structures (Xu and He 2017). Besides the intervention and repair cost examined in previous studies, downtime of either a portion or the entire building should be considered in relation to life-cycle performance analysis. This analysis can precisely evaluate the initial investment decision by stakeholders that will be needed for tall buildings.

Theoretical Background

Parent and Extreme Wind Speed Distribution in a Mixed Climate

The prediction of wind hazards, such as hurricanes and thunderstorms, is a subfield of meteorology. Because these weather phenomena threaten structural safety and integrity, prediction of these hazards and estimation of their intensity are always the first steps in a PBWE analysis. Currently, there are few models able to quantify the probabilistic wind speeds for a given structure, but those that exist are discussed in this paper.

The first model is designated as parent wind speed distribution. It uses hourly records extracted from a historical database of wind speeds from a meteorological station located in the proximity of the structure (Seo and Caracoglia 2013; Cui and Caracoglia 2015). The advantage is that wind speed records are reliable; a large number of weather stations (NOAA 2015) can cover most of the United States. However, the weather recording "memory" is relatively short compared with the typical life cycle of a structure (between 50 and 100 years); in addition, the database is deficient in the case of hurricane winds. Therefore, the yearly extreme mean-wind speed distribution is developed to analyze extreme wind speeds and is used to extrapolate the longer times (50–100 years) and the design wind speeds. Parent mean-wind speed distribution is widely used to calculate buildings' serviceability performance, such as pedestrian wind microclimate (Lawson 1978) against periodic moderate wind speed events. The wind speed distribution of the yearly maxima is used to evaluate building key functions and failure probability, such as operating conditions of elevators and facades.

Besides more frequent extra-tropical winds events, hurricanes, which are rare but intense, are normally simulated by numerical methods (Vickery et al. 2009). This synthetic simulation of hurricanes uses historical records to identify the main patterns of the wind events and subsequently generate synthetic hurricane wind speed records. The benefit of this method is that the numerical simulation can generate a large number of wind hazard events; it is also reliable because it is derived from (and can be validated by) actual historical records.

Traditionally, the wind speed probability distribution of both parent and yearly extreme wind speeds can be approximately modeled using a Weibull model (Cui and Caracoglia 2016). Recently, the joint probability density function (PDF) of the reference mean-wind speed and direction has been examined in wind engineering to accurately evaluate the local microclimate effects on structures (Cui and Caracoglia 2018b; Ciampoli and Petrini 2012; Barbato et al. 2013; Xu et al. 2009; Petrini et al. 2011). In the meteorological science field, the joint PDF of wind speed and direction can be modeled by an angular-linear distribution (Carta et al. 2008)

$$f(U,\theta) = 2\pi g(\zeta_g) f_U(U) f_\Theta(\theta); \quad 0 \le \theta \le 2\pi; \quad 0 < U < \infty \tag{1}$$

where f_U = marginal PDF of U mean wind speed at a reference height; f_Θ = marginal PDF of θ mean wind direction; and $g(\zeta_g)$ = PDF of the circular variable ζ_g.

Frequency Domain Analysis of a Tall Building Response

For serviceability limit conditions, which are usually predominant in the wind-resistant design of a tall building, a linear elastic structural model is adequate (Davenport 1988), and the standard frequency domain random vibration analysis of the Davenport chain can be used if the stationary wind load hypothesis is used (Davenport 1971).

The study by Cui and Caracoglia (2018a) proposes an analytical solution for the dynamic response, induced by multidirectional winds, with coupled structural modes shapes. The fundamental generalized dynamic scalar modal equation for mode j in the dimensionless frequency domain is

$$\frac{8m_j\pi^2}{\rho D^4 h}[f_j^2 + 2\xi_j f_j \iota f - f_j^2]\hat{\chi}_j(f) + \sum_{k=1}^{N}[s_{j,k} + \iota f c_{j,k}]\hat{\chi}_k(f) = q_j \tag{2}$$

where m_j = modal mass; D and h = building reference width and height; $f = nD/U_h$ = normalized frequency; $f_j = j$th modal frequency; $s_{j,k}$ and $c_{j,k}$ = elements of stiffness and damping matrices; q_j = modal wind force; and $\hat{\chi}^j$ = modal displacement in the frequency domain.

The double integral used to evaluate wind loads on tall buildings can be replaced by high-frequency force balance (HFFB) experimental results from wind tunnel tests (Chen and Kareem 2005); coupled intermodal effects can also be considered using HFFB results (Cui and Caracoglia 2017).

Proposed Life-Cycle Downtime Estimation Methodology

Out-of-service downtime has rarely been included in loss analysis for tall buildings. The importance of wind load–induced, out-of-service downtime should be emphasized and analyzed in parallel with the intervention cost estimation.

Before describing the out-of-service downtime estimation methods for tall buildings, similarities and differences compared with wind-induced damage are discussed. For example, building's damaged elements after an extreme wind event are associated with different out-of-service downtimes, during which inspection and repair are needed to restore the structure to its initial condition. Furthermore, a minor wind hazard may interfere with tall building services, such as habitability of upper floors, without causing any damage.

Therefore, wind-induced interruptions are classified into two categories: (1) frequent events where out-of-service time is related to the duration of the wind event only because it is related to residents' comfort; and (2) extreme events where part or the entire building system is out of service and the repair or intervention time

after the end of the extreme wind event can be assumed as a constant number.

Minor wind-induced interruptions usually occur more frequently (>1 times per year), and the total annual downtime resulting from temporary inhabitability is estimated through the parent wind speed distribution. Severe, extreme wind hazards are much less frequent and the extreme wind speed distribution is used to compute the annual failure probability.

The life-cycle, out-of-service downtime estimation formula can be derived from the life-cycle cost estimation formula in Eq. (3)

$$E[T(t)] = \sum_{k=1}^{t} 8766 \int_0^{2\pi} \int_0^{\infty} r(\theta, U_h) f_p(\theta, U_h) dv d\theta + E\left[\sum_{i=1}^{N(t)} \left(\sum_j T_j P_j\right)\right] \quad (3)$$

$$P_j = \int_0^{2\pi} \int_0^{\infty} F_j(\theta, U_h) f_e(\theta, U_h) dU_h d\theta \quad (4)$$

Eq. (3) has two parts. In the first part, $T(t)$ = total out-of-service time in hours at time t (years); k = sequential counting index during a life cycle; $f_p(\theta, U_h)$ = distribution of the parent hourly wind speeds and directions; $r(\theta, U_h)$ = ratio of the out-of-service area with respect to the whole building floor area for various wind speeds U_h and directions θ; and 8,766 = average total hours in 1 year. In the second part, T_j = restoration time needed for damage category j; P_j = damage probability for category j during one wind event; and $N(t)$ = total number of wind events from initial time to time t. Eq. (3) can be simplified to obtain the relative downtime, which is the expected out-of-service time normalized with respect to the total hours for each year (8,766), as

$$E[\Gamma(t)] = \sum_{k=1}^{t} \int_0^{2\pi} \int_0^{\infty} r(\theta, U_h) f_p(\theta, U_h) dv d\theta + E\left[\sum_{i=1}^{N(t)} \left(\sum_j \gamma_j P_j\right)\right] \quad (5)$$

where γ_j is the ratio between the out-of-service time for the jth damage category and the total hours per year ($\gamma_j = T_j/8{,}766$).

For illustration purposes, a total of three wind-induced interruptions, corresponding to different damage categories, are considered and shown in Fig. 1:

- Acceleration causing occupants' discomfort. Discomfort (motion sickness) is normally induced by large accelerations, which are more frequent than other wind damages and may occur several times during a year. The inhabitable space should temporarily be closed during wind hazards, but no building elements will be damaged.
- Key equipment failure ($j = 1$). During severe wind hazards, some building equipment or elements may be damaged by wind-induced vibration or falling objects. The key equipment failure can prevent the operations of the whole building. In this paper, electric equipment failure at a midlevel floor of a tall building is considered to affect the whole building operations in terms of global downtime.
- Facades damaged by flying debris ($j = 2$). External flying debris during wind events may damage building facades, usually affecting several lower-level floors rather than the whole building's lateral surface area (Moghim and Caracoglia 2012).

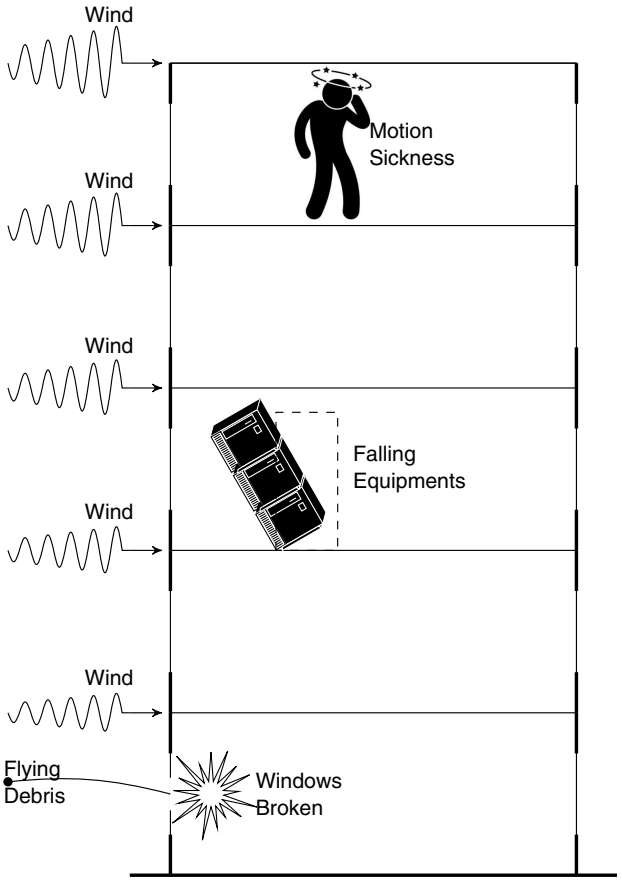

Fig. 1. Wind-induced damage categories (examples) in a tall building with different recurrence intervals.

As a result, this related downtime should be calculated accordingly.

In summary, the prediction of lifetime monetary and out-of-service losses is composed of a total of five steps, as also illustrated in Fig. 2:

1. Modeling of parent wind speed and direction joint probability distribution $f^p(\theta, U_h)$, which is derived from historical records of weather stations;
2. Modeling of extreme wind speed and direction joint probability distribution $f^e(\theta, U_h)$. In hurricane-prone areas, these extreme winds are derived from synthetic hurricane simulations;
3. Evaluation of fragility curves for each wind damage category F_j;
4. Estimation of the inhabitable space $A(\theta, U_h)$ for different combinations of wind speed U_h and direction θ; and
5. Out-of-service downtime prediction over structural lifetime.

Application of Life-Cycle Downtime Estimation Methodology

Experimental Errors and Fragility Curves

To demonstrate the feasibility of the proposed framework, an application example is presented in this section. The benchmark structure used in this study is the Commonwealth Advisory Aeronautical Research Council (CAARC) tall building (Melbourne 1980). The wind-induced building response for different mean wind speeds U_h and mean wind directions θ is calculated by Eq. (2) in section "Theoretical Background," which has been

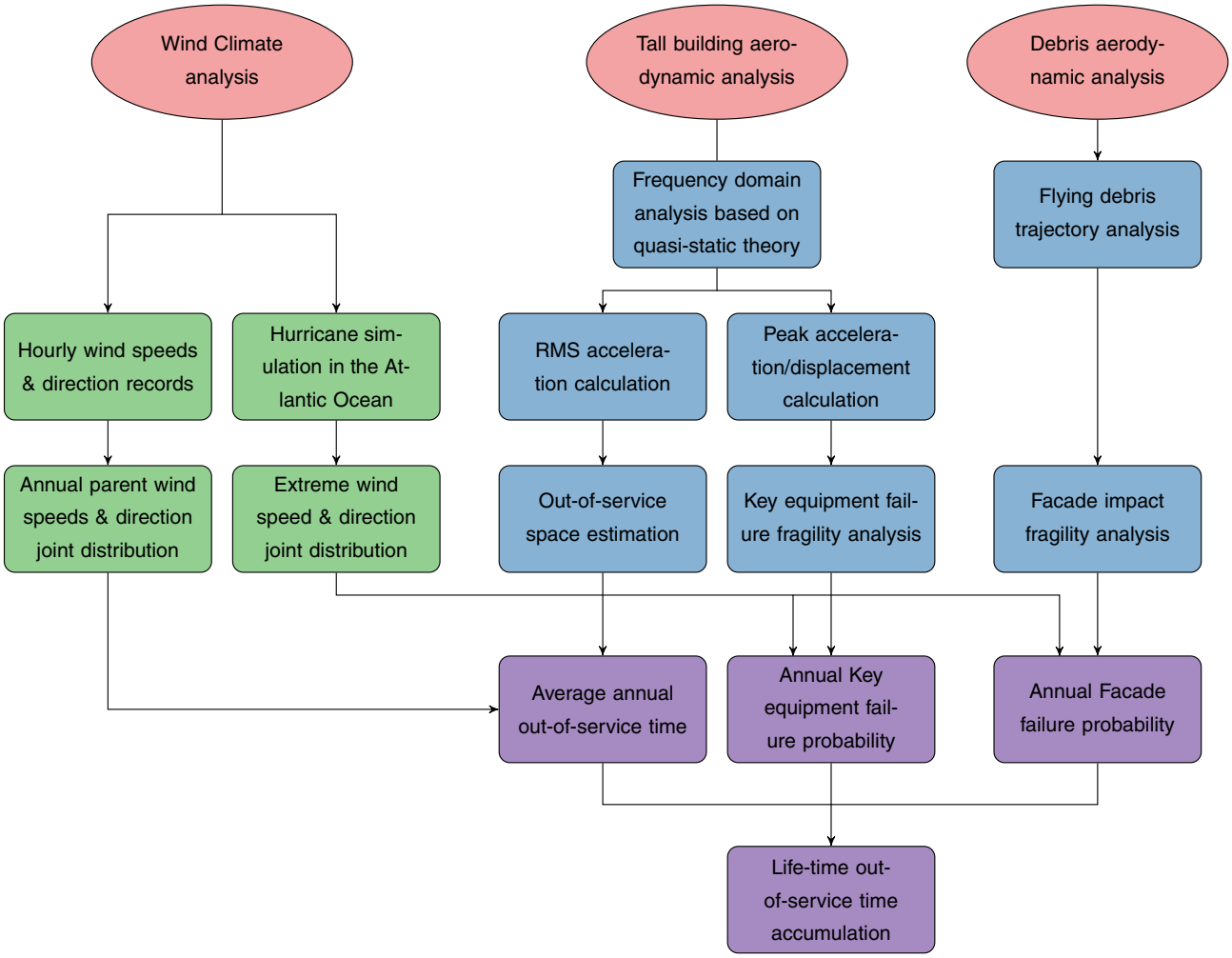

Fig. 2. Flow chart of structural life-time cost and downtime estimation methodology.

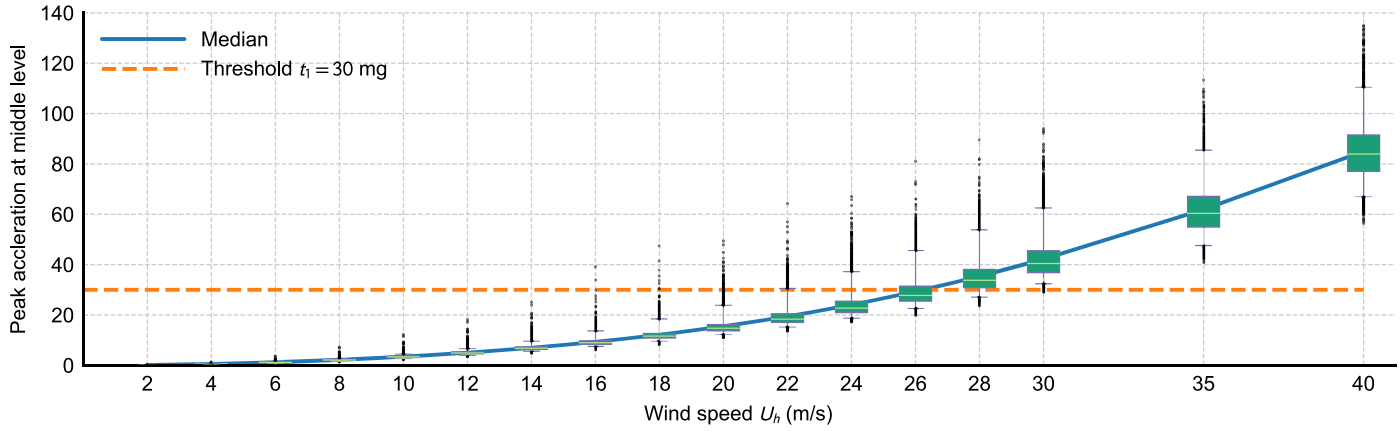

Fig. 3. CAARC midlevel peak acceleration variance when $\theta = 0°$.

verified in a previous study (Cui and Caracoglia 2018a). The quantity U_h is estimated at the building rooftop.

Fragility Curves for Key Equipment Failure

Acquisition of a large wind load data set is needed to identify various uncertainty sources (and parameters). Moreover, using several uncertain parameters and non-uniplanar, coupled structural mode shapes drastically increases the computing time needed for calculating the generalized modal forces (Smith and Caracoglia 2011) and hinders the implementation of rigorous methods for aeroelastic uncertainty propagation, such as stochastic calculus (Caracoglia 2014). For these reasons (Cui and Caracoglia 2017), three

simplified formulas are proposed to quantify and simulate the experimental errors associated with HFFB experimental measurements in a wind tunnel. Ultimately, these errors will be propagated into the structural fragility curves for various damage categories through the structural response theory in the section "Theoretical Background."

In this study, key equipment is assumed to be located at the tall building's midlevel floor and will be damaged if the peak acceleration threshold $t_1 = 30$ mg is exceeded (Hwang et al. 2004). The peak acceleration threshold depends on the equipment's configuration and needs to be re-evaluated case by case. Because of wind tunnel experimental errors, uncertain wind loads are measured on a tall building model, causing wind-induced acceleration variances on the key equipment. A total of 5,000 random wind-related uncertain HFFB parameters are generated, using the empirical generalized-load PSD model and the Copula method (Cui and Caracoglia 2017); the wind-induced accelerations at the middle-floor level are calculated by Monte Carlo method.

For example, the box plot in Fig. 3 illustrates the acceleration variations caused by the wind tunnel-related parameter uncertainty. For each wind speed, the middle white line corresponds to the median acceleration and is connected by a dark solid line; the rectangular boxes show the 25th and 75th percentiles of accelerations; the whiskers present the 2.5th and 97.5th percentiles; and the data scatter suggests some outliers outside of the whiskers. When the wind speed increases, both the mean value and the variations of acceleration drastically increase. When the wind speed at the reference rooftop elevation U_h is below 20 m/s, zero or few cases exhibit exceedance of the predefined threshold; thus, the key equipment at midlevel floors is secure. When $U_h > 30$ m/s, almost all accelerations associated with parameter variability are beyond the threshold; therefore, the key equipment is very likely to be damaged. When 20 m/s $< U_h <$ 30 m/s, the damaging events of the key equipment are uncertain, and the damage probability is determined by U_h and the variance of the random parameters (Cui and Caracoglia 2015).

After combining all the exceedance probability results $P_1(\theta, U_h)$, which are conditional on the mean wind speed at the rooftop U_h and mean wind incidence angle θ, the fragility surface of the key equipment is found in Fig. 4 for $j = 1$. Because the mean wind direction is an angular variable, the fragility surface is plotted using polar coordinates. Because of the symmetrical floor plan of the CAARC, the fragility surface is only plotted when the relative mean wind incidence angle is $0 \le \theta \le 90°$. Examination of Fig. 4 suggests that, besides the wind speed, the probability of exceeding the limit state threshold $t_1 = 30$ mg also depends on the relative wind direction. For intermediate values of the wind speed, the probability around the relative wind direction $\theta = 45°$ is lower than that found for other relative wind directions. This observation confirms the relevance of a comprehensive multidirectional wind load analysis.

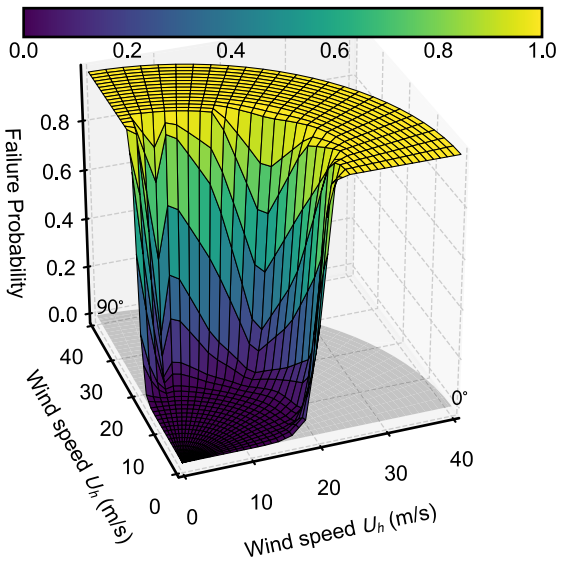

Fig. 4. Fragility curve of the key equipment failure at a midlevel floor of the CAARC building.

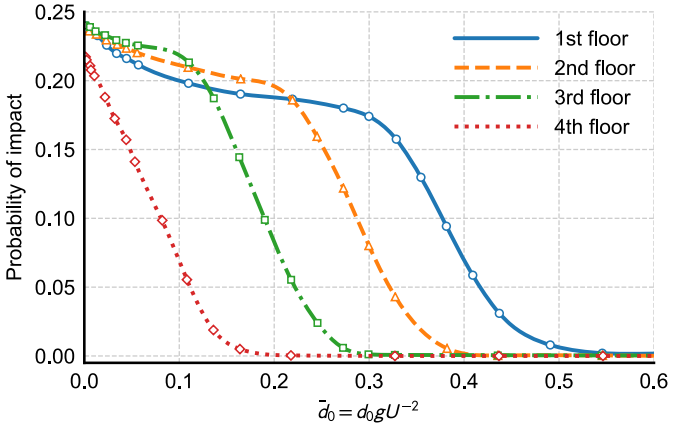

Fig. 5. Probability of impact $P_d(\bar{d}_0)$ against the facade of the CAARC building as a function of $\bar{d}_0 = d_0 g/U^2$ for a standard-size window (or cladding element).

Fragility Curves for Facades

Besides the key equipment failure, another important wind-induced failure on the facade is caused by flying debris. In Moghim and Caracoglia (2012), a dimensionless universal probability curve is used to describe the debris impact probability against a window or a cladding element of unit depth (width) and height equal to the interstory height, as a function of the dimensionless quantity $\bar{d}_0 = d_0 g/U^2$. In this expression, g is the gravity acceleration; d_0 is the distance between debris source and target building windows/cladding; and U is a reference mean wind speed. This study uses the general fragility curves $P_d(\bar{d}_0)$ in Fig. 5 for the first floor to the fourth floor from a previous study (Moghim and Caracoglia 2012).

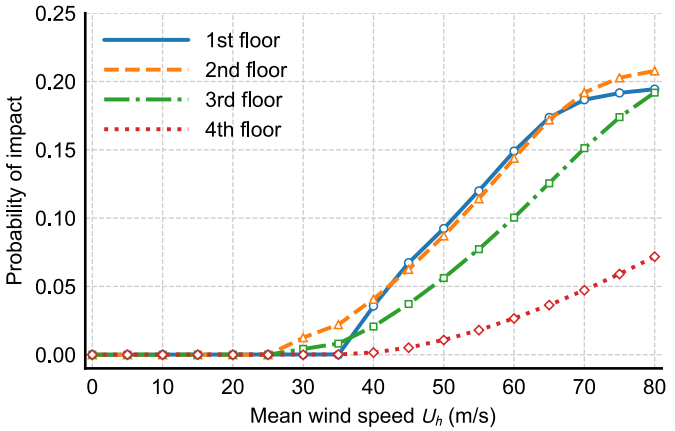

Fig. 6. Fragility curves of the CAARC building for the limit state of debris impact against the vertical facade at the first floor to fourth floor.

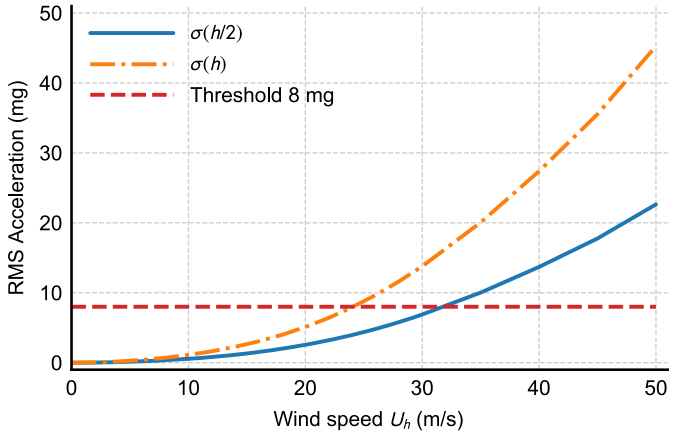

Fig. 7. RMS accelerations at a midlevel floor and roof-top level for wind direction $\theta = 0°$.

Other upper floors are assumed to have no flying debris damage. As explained by Moghim and Caracoglia (2012), in a typical urban setting, where most surrounding buildings are medium rise (i.e., the sources of debris cannot exceed heights above 20–30 m), only the first four floors can be considered for debris effect. Even though damage is also possible on higher floors (Jain 2013, 2015), this condition is usually associated with site-specific characteristics and a unique building orientation. Therefore, as a first approximation, the approach recommended by Moghim and Caracoglia (2012) can be used. The model parameters are also found from the literature (Moghim and Caracoglia 2012). Because of the complex aerodynamics of flying debris, there is still no clear consensus on how to model turbulence and directionality effects on the flying debris trajectory (Moghim and Caracoglia 2012). Thus, the wind direction is conservatively assumed to be perpendicular to the main vertical facade surface.

When determining vulnerability to debris impact, the debris source condition and the boundary layer effect within the wind field should be considered. During extreme wind hazards, the debris is often generated from nearby residential areas. Consequently, the probability of window impact should include the distribution of possible debris sources from nearby areas

$$P_{2,i}(U_h) = \int_A f(d_0) P_d(d_0, U_i) dd_0 \tag{6}$$

In Eq. (6), $P_{2,i}(U_h)$ = second category (facade) failure at the ith floor for mean wind speeds U_h at reference height $z = h$; A = debris source area; and U_i = mean wind speeds at the ith floor, using $U_i = U_h(z_i/h)^{0.28}$ to simulate Category B roughness exposure in ASCE 7 (ASCE 2016).

One preliminary, simplified example is considered in this study. The debris source is uniformly distributed [i.e., $f(d_0)$] around the CAARC building between $d_0 = 10$ m and $d_0 = 60$ m; the average height of the debris source can be found in Moghim and Caracoglia (2012).

After integrating the debris source probability, the damage probability for different wind hazard intensities can be calculated using Eq. (6) and the dimensionless fragility in Fig. 5. The results (fragility curves) are plotted in Fig. 6.

Inhabitable Area Ratio

Unlike the previously discussed wind-induced damage, inhabitable living space in a tall building during a high-wind event may occur frequently, but normal conditions are restored immediately after the event. Therefore, the same method used to evaluate the exceedance probability in the previous subsections for the two damage categories cannot be applied. A new quantity, inhabitable area ratio $r(\theta, U_h)$, is proposed in this subsection to describe the different wind intensities and their effects on the tall building habitability.

For one set of experimental parameters, the tall building's root-mean square (RMS) accelerations at rooftop level $\sigma_a(h)$ and at a midlevel floor $\sigma_a(h/2)$ can be calculated using the frequency domain analysis theory in the section "Theoretical Background." For example, when the wind direction is 0°, $\sigma_a(h)$ and $\sigma_a(h/2)$ are plotted in Fig. 7 with the predefined occupants' discomfort threshold equal to 8 mg (Cui and Caracoglia 2015; Kwok et al. 2009). If the mode shape is linear along the height (shear-type building), the RMS acceleration should increase linearly with elevation and, the highest elevation $z_{8\ \mathrm{mg}}$ below the threshold can be found using linear interpolation or extrapolation. Therefore, the inhabitable area ratio is

$$r(\theta, U_h) = \frac{h - z_{8\ \mathrm{mg}}}{h} = \frac{\sigma_a(h) - 8\ \mathrm{mg}}{2[\sigma_a(h) - \sigma_a(h/2)]}\bigg|_{\theta, U_h} \tag{7}$$

Next, the distribution of $r(\theta, U_h)$ for certain wind speeds and directions can be found using Monte Carlo sampling methods. Fig. 8 illustrates the mean and box plot of $r(\theta, U_h)$ using a sample of 5,000 Monte Carlo simulations when $\theta = 0°$. The definition of the median line, boxes, whiskers, and scatter points are the same as in Fig. 3. Fig. 8 suggests that, when $U_h < 20$ m/s, zero or few outliers have non-zero inhabitable area ratio, and when

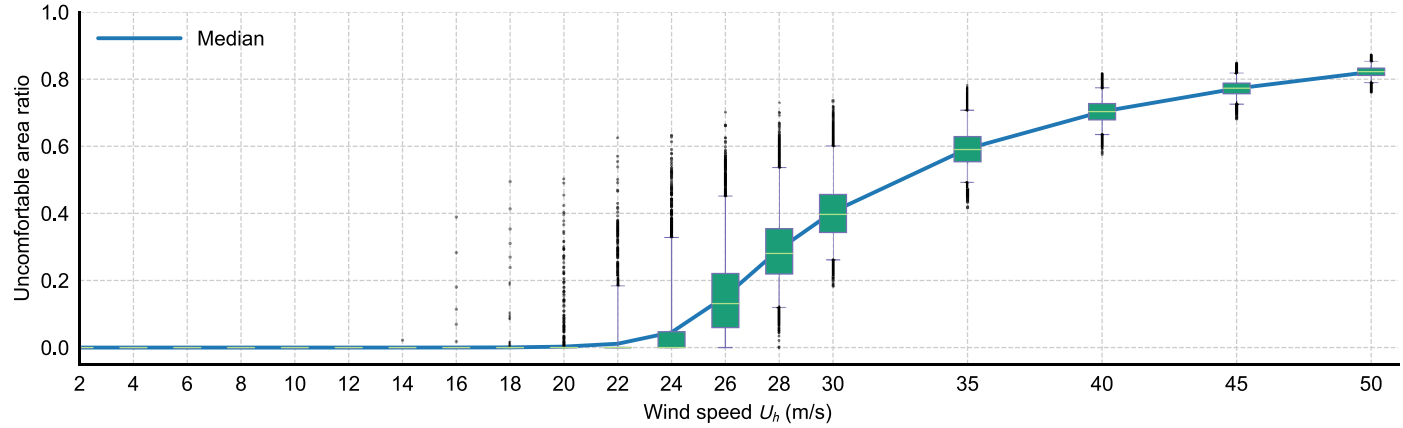

Fig. 8. CAARC's inhabitable-area ratio variability at various wind speeds when $\theta = 0°$.

$U_h > 40$ m/s, the inhabitable area ratios are mostly around 0.8. For 20 m/s $< U_h <$ 40 m/s, both mean value and standard deviation vary as wind speeds increase, which demonstrating that the uncertainty effect caused by experimental errors cannot be ignored for acceleration-induced comfort problems.

By combining mean inhabitable area ratio results at various wind speeds and directions (θ, U_h), $r(\theta, U_h)$ is obtained and plotted in Fig. 9. Similar to Fig. 4, for the same the wind speed the probability values around the relative wind direction ($\theta = 45°$) are lower than those found for other relative wind directions.

Wind Climate of the Target Site

After determining the fragility curve/surface for various damage categories and the mean inhabitable area ratio, the life-cycle analysis of a specific building performance objective against wind hazards must consider the local wind climate data at the building site. For rare and extreme wind speed events, the fragility curve/surface must be multiplied by the extreme wind speed probability distribution to determine the failure probability during one wind event. Conversely, for frequent wind events, the parent wind speed distribution should be combined with the mean inhabitable area ratios to calculate an annual discomfort duration.

In this section, the CAARC tall building is assumed to be located in Miami, Florida, which has a typical tropical monsoon (mixed) climate; wind climate analysis procedures and results follow.

Parent Wind Speeds

The hourly wind speed data records are derived from the integrated surface database at meteorological station 722020 maintained by the National Oceanic and Atmospheric Administration (NOAA). This station is located at the Miami International Airport; the anemometer is installed 10 m above ground. Fig. 10 illustrates the wind rose according to records from 1973 to 2017 with 429,365 data entries. The wind directions, shown in Fig. 10, clearly suggest that there two monsoon patterns in Miami: easterly and northwesterly. The original NOAA data may consist of hurricane-related winds speeds; however, the proportion is less than 1%. Consequently, the hurricane-related wind data will not affect the derivation of the overall parent wind speed distribution.

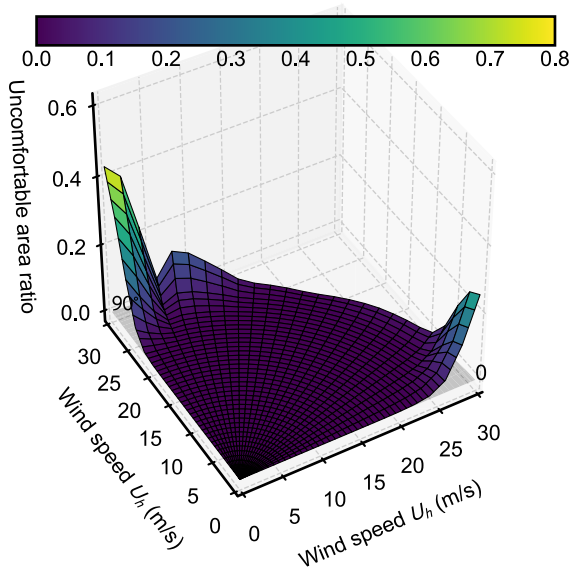

Fig. 9. Mean values of CAARC's inhabitable-area ratios for different wind speeds U_h and wind directions θ.

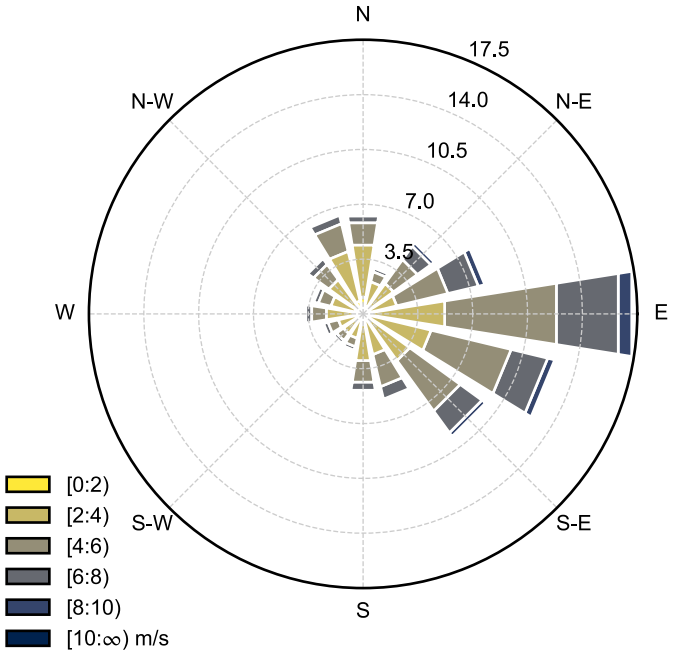

Fig. 10. Wind rose of hourly speed and direction records at $z = 10$ m in Miami, Florida (%).

In the previous section, the wind speed was defined as U_h at the reference height $z = h$. Normally, the region surrounding an airport can be considered as open terrain; therefore, the boundary-layer power law can be used to convert wind speeds from 10 m to h, and $U_i = U_h(z_i/h)^{0.28}$ according to Category B exposure of ASCE 7 (2016). Therefore, the marginal wind speed distribution and marginal wind direction distribution are presented in Figs. 11 and 12, respectively. In Fig. 11, the Weibull distribution can fit fairly well the empirical histogram of the parent wind speeds (Simiu and Scanlan 1996). Because there are two patterns in the wind directions, the wind direction histogram is fitted using the mixture Von Mises distribution with $N_m = 2$ (Carta et al. 2008). After combining the wind speed and wind direction distribution using the

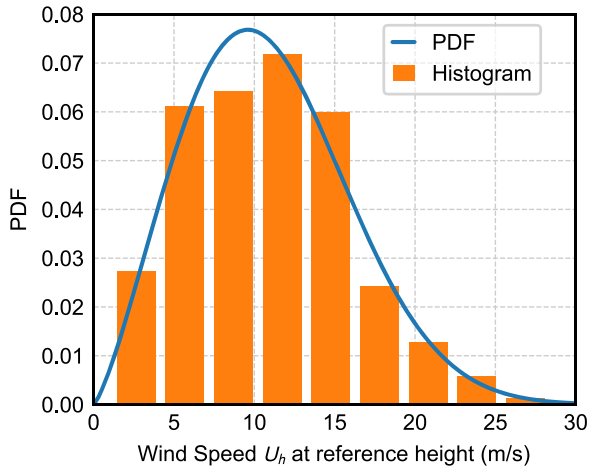

Fig. 11. Distribution of marginal parent mean wind speed U_h.

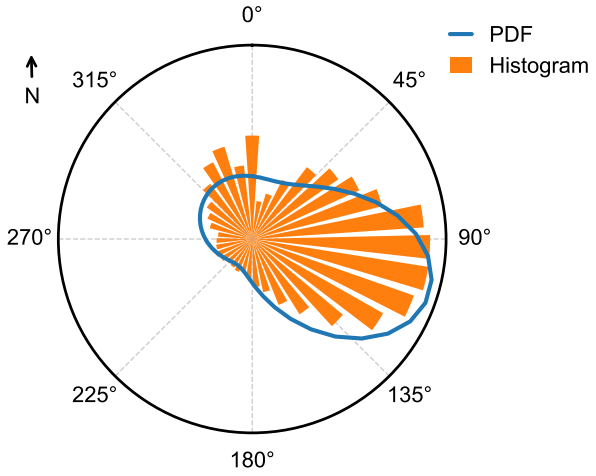

Fig. 12. Distribution of marginal parent mean wind direction θ.

angular-linear distribution formula in Eq. (1), the joint PDF of wind speed and direction is calculated and illustrated in Fig. 13.

Hurricane Extreme Wind Speeds

In extra-tropical wind climate environments, the extreme wind speed distribution can be modeled by the maximum wind speed records per epoch or per wind event based on the extreme value distribution model (Simiu and Scanlan 1996). However, in hurricane-prone regions, the extreme wind events are usually caused by hurricanes. The hurricane landing occurrence rates and intensity considerably vary each year. A relatively short observation period (a few decades of meteorological data) is not sufficient to accurately predict the extreme wind speeds. Vickery et al. (2000) developed a synthetic hurricane simulation method in a series of studies. Inspired by this method, Cui and Caracoglia (2019) proposed a simplified, equivalent simulation method. Twenty thousand years of synthetic simulation results are used in this study to determine the distribution of the gradient wind speeds, originating from hurricanes landing in the influence region around Miami. Results are plotted in Fig. 14.

Fig. 14 exhibits a completely different pattern in comparison with the parent wind rose in Fig. 10. The directions associated with

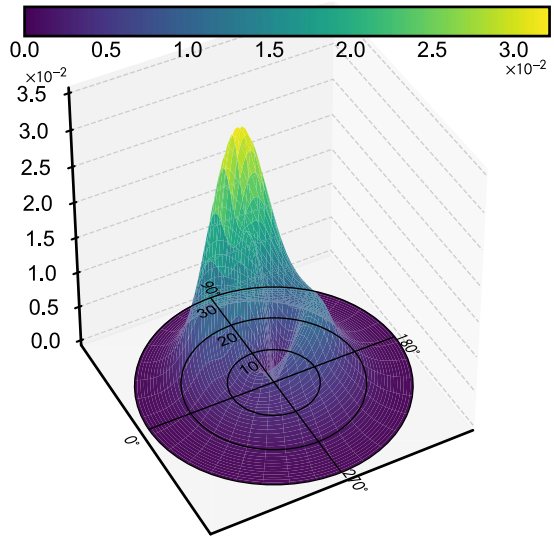

Fig. 13. Joint PDF of parent wind speed and direction.

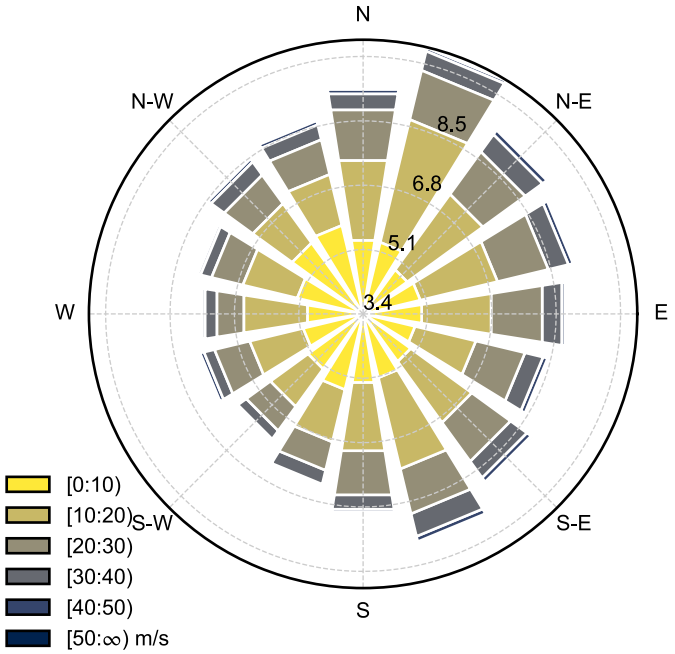

Fig. 14. Wind rose of annual extreme hurricane wind speeds at gradient height and directional simulation results for Miami, Florida (%).

extreme wind speeds are distributed more uniformly because the wind directions at hurricane landing are determined by more factors, such as the relative position between the hurricane center and building site and the hurricane translation speed and direction (Vickery and Twisdale 1995). Because most hurricane paths near the Florida peninsula are aligned in the east-west direction, the northerly and southerly winds are slightly more frequent than those associated with other directions.

Similar to the parent wind, the annual extreme wind speeds caused by hurricanes must be converted to the reference height $z = h$. After this conversion (Batts et al. 1980), the final empirical probability distribution and fitted Weibull distribution are presented in Fig. 15. The marginal wind directions distribution and joint distribution of wind speed and direction are analyzed by the same methods as that used for parent wind speeds. Results are illustrated in Figs. 16 and 17.

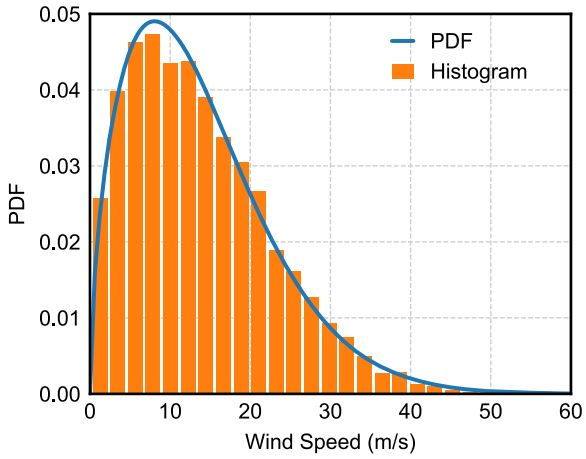

Fig. 15. Marginal distribution of annual extreme wind speed U_h, originating from hurricanes (Miami, Florida).

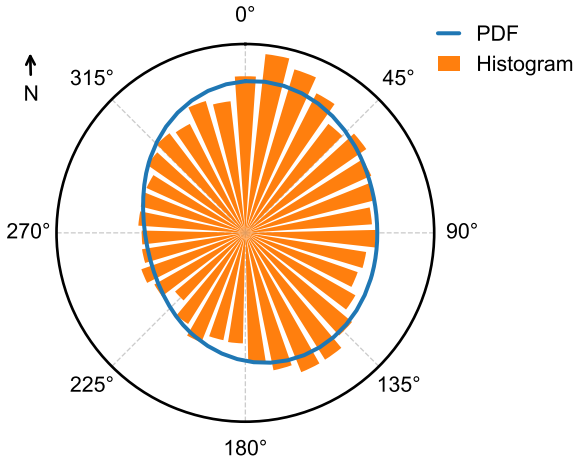

Fig. 16. Marginal distribution of annual extreme wind direction θ, originating from hurricanes (Miami, Florida).

Downtime Prediction and Discussion

Because structural performance and fragility depend on wind direction, one extra parameter should be introduced to define building orientation: Ω (Fig. 18) (i.e., the angle between the direction of x local coordinate axis and the north direction).

As explained in the section "Proposed Life-Cycle Downtime Estimation Methodology," the CAARC benchmark tall building downtime analysis includes three parts: (1) discomfort to residents caused by large accelerations, (2) whole building shutdown caused by key equipment failure, and (3) partial building shutdown caused by windborne debris damage on external facades.

Because the acceleration-induced inhabitability of residential areas is more frequent and downtime does not usually extend beyond the duration of the specific wind event, downtimes can be directly related to the duration of the strong wind event. If the wind climate and structural dynamic properties remain the same over the building life cycle, this annual downtime T_p, in years, can be considered constant

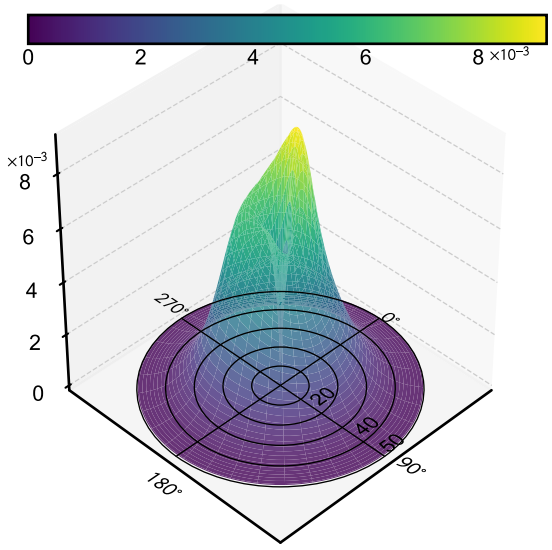

Fig. 17. Joint PDF of annual extreme wind speed and direction, originating from hurricanes.

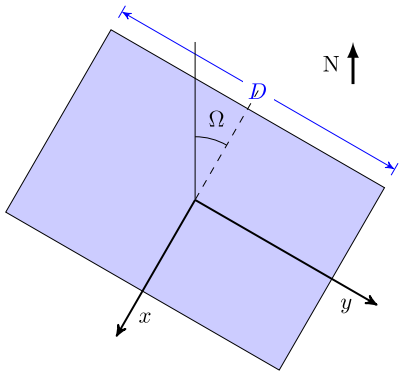

Fig. 18. Schematic of CAARC building's orientation (top view).

$$T_p(\Omega) = \int_0^{2\pi} \int_0^{\infty} r(\theta + \Omega, U_h) f_p(\theta, U_h) dv d\theta \qquad (8)$$

Because $r(\theta, U_h)$ is the inhabitable area ratio and $f_p(\theta, U_h)$ is the parent wind distribution, T_p can be interpreted as an annual equivalent building downtime resulting from the acceleration limit state. Using the $r(\theta, U_h)$ and $f_p(\theta, U_h)$ calculated in the previous section, $T_p(\Omega)$ can be calculated for various building orientations by Eq. (8), as illustrated in Fig. 19.

Conversely, the wind damage caused by extreme winds is usually associated with hurricane events. The downtime caused by failures of key equipment and damage to facades is related to the extreme wind speeds and directions of each hurricane. Annual hurricane landing rate is random, which is modeled as a Poisson process (Mudd et al. 2014). For the region surrounding Miami, the mean annual hurricane influence (arrival) rate is 6.08, which is chosen as the Poisson process parameter λ. The hurricane influence region is the whole hurricane region with wind speeds larger than 0, which is a region much larger than the hurricane landing area. Thus, the hurricane influence rate is greater than the annual landing rate in Vickery et al. (2000). A population of 5,000 samples is used to compute the mean life-cycle downtime, resulting from the two building damage categories, by Monte Carlo sampling.

If the downtime is assumed as $T_1 = 168$ h and $T_2 = 24$ h for the two damage categories, the life-cycle accumulated downtime

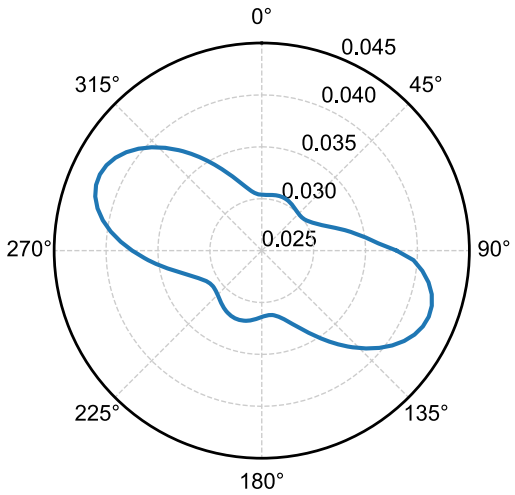

Fig. 19. Annual equivalent whole-building inhabitability downtime resulting from acceleration (year).

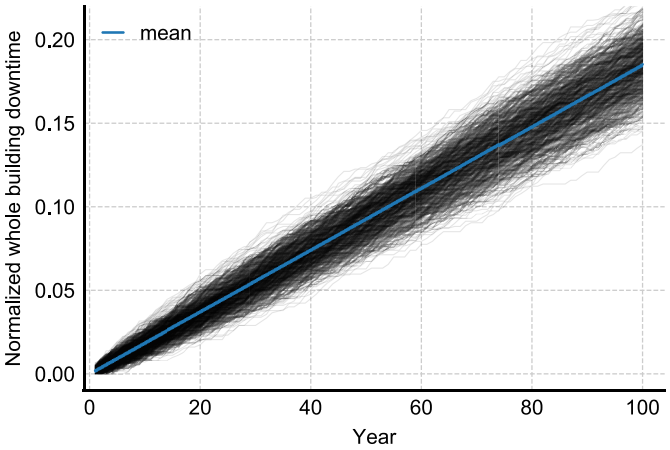

Fig. 20. Normalized life-cycle downtime accumulation for key equipment failure when $\Omega = 0°$.

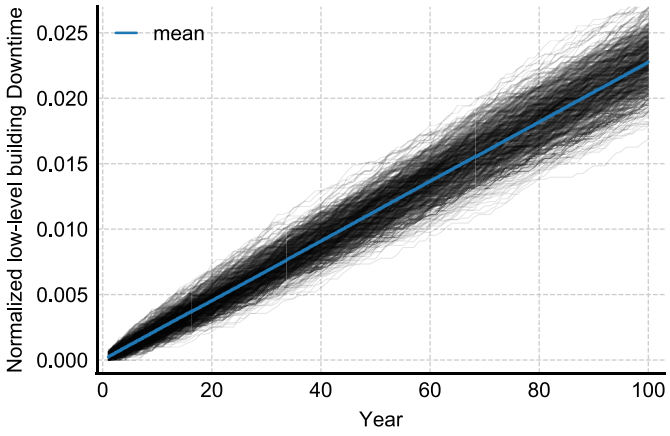

Fig. 21. Normalized life-cycle downtime accumulation for wind-borne debris damage to facades.

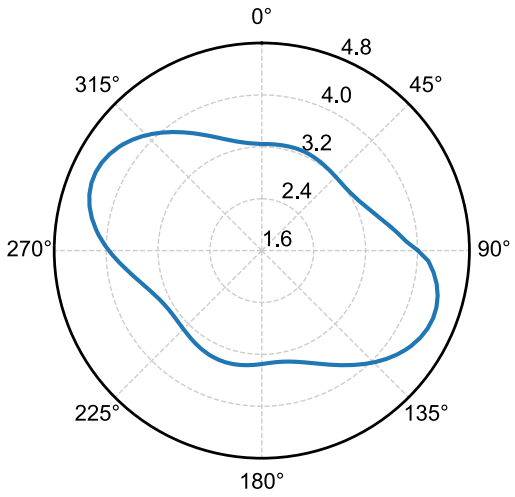

Fig. 22. Normalized life-cycle downtime accumulation after $t = 100$ years.

for the two previously defined categories is presented in Figs. 20 and 21, when the building orientation is $\Omega = 0°$ (north direction parallel to D vertical face). In these two figures, the downtime is normalized to hours per year. The thin, light-colored and continuous lines are downtime accumulations for each sample. Every increment over time is random because of the hurricane landing process. Nevertheless, because the hurricane landing rate is simulated by a stationary Poisson process, the mean life-cycle downtime linearly increases over time. For the damage caused by debris on vertical facades, the downtime is approximately estimated as 24 h if windows on any floors are damaged. Because the wind direction is excluded in debris trajectory analysis, the downtime for Damage category 2 is independent of θ.

Combining all the wind-induced damage categories, the total downtime in years at the end of the life cycle ($t = 100$ years) for various building orientations Ω is presented in Fig. 22. Comparing Fig. 19 with Fig. 22, the downtime dependency on wind direction is similar; furthermore, the acceleration-induced downtime is the main component of this accumulation.

Conclusions

This paper proposes a framework and a numerical method to estimate tall building life-cycle downtime, which extends the application of performance-based wind engineering to serviceability evaluation. The CAARC tall building, located in the hurricane-prone area of Miami, Florida, is used as the benchmark structure in this study. Similar to previous work by the authors, the framework can be divided into sequential modules.

Three wind-induced inconveniences and related downtime durations were considered: excessive acceleration causing discomfort to occupants and key equipment failure, cracked/broken cladding components, and windows hit by flying debris. First, the wind climate information was described by two separated probabilistic models: parent wind distribution and extreme wind distribution. The former was derived from climate database records available at a nearby methodological station; the latter was computed from synthetic hurricane simulations. Second, because the tall building downtime is caused by frequent low-intensity wind load events characterized by parameter variability, aerodynamic load uncertainties were included in the analysis. Therefore, records from repeated wind tunnel tests on a scale model of the CAARC building were used to evaluate the multidirectional wind effects on the full-scale benchmark building, along with projected debris trajectories accounting for experimental errors. Third, the downtime accumulation over the structural lifetime, caused by both extra-tropical winds and extreme hurricane winds, were assessed from failure probabilities. In summary, this study provides a unified, novel solution to examine the wind-induced building downtime and to evaluate structural performance of tall buildings against wind-induced damage in hurricane-prone regions of the United States.

Acknowledgments

This research was supported in part by the National Science Foundation of the United States of America under CAREER Grant No. CMMI-0844977 during 2009–2014. The partial support of NSF Grant No. CMMI-1434880 is also acknowledged during 2014–2018. Finally, the sponsorship of Shanghai Pujiang Program (No. 19PJ1409800) is acknowledged. Any opinions, findings, and conclusions or recommendations are those of the authors and do not necessarily reflect the views of the sponsors.

References

ASCE. 2016. *Minimum design loads for building and other structures*. ASCE 7. Reston, VA: ASCE.

Barbato, M., F. Petrini, V. U. Unnikrishnan, and M. Ciampoli. 2013. "Performance-based hurricane engineering (PBHE) framework." *Struct. Saf.* 45 (Nov): 24–35. https://doi.org/10.1016/j.strusafe.2013.07.002.

Batts, M. E., E. Simiu, and L. R. Russell. 1980. "Hurricane wind speeds in the United States." *J. Struct. Div.* 106 (10): 2001–2016.

Bernardini, E., S. Spence, M. Gioffrè, and A. Kareem. 2012. "A reliability approach for the wind-induced response assessment of tall buildings using the high frequency force balance." In *Proc., 7th Int. Colloquium on Bluff Body Aerodynamics and Applications (BBAA7)*, 825–834. Beijing: China Communications Audio-Visual & Electronic Press.

Bernardini, E., S. M. Spence, and A. Kareem. 2013. "A probabilistic approach for the full response estimation of tall buildings with 3D modes using the HFFB." *Struct. Saf.* 44 (Sep): 91–101. https://doi.org/10.1016/j.strusafe.2013.06.002.

Caracoglia, L. 2014. "A stochastic model for examining along-wind loading uncertainty and intervention costs due to wind-induced damage on tall buildings." *Eng. Struct.* 78 (Nov): 121–132. https://doi.org/10.1016/j.engstruct.2014.07.023.

Carta, J. A., P. Ramírez, and C. Bueno. 2008. "A joint probability density function of wind speed and direction for wind energy analysis." *Energy Convers. Manage.* 49 (6): 1309–1320. https://doi.org/10.1016/j.enconman.2008.01.010.

Chen, X., and A. Kareem. 2005. "Dynamic wind effects on buildings with 3D coupled modes: Application of high frequency force balance measurements." *J. Eng. Mech.* 131 (11): 1115–1125. https://doi.org/10.1061/(ASCE)0733-9399(2005)131:11(1115).

Ciampoli, M., and F. Petrini. 2012. "Performance-based Aeolian risk assessment and reduction for tall buildings." *Probab. Eng. Mech.* 28 (Apr): 75–84. https://doi.org/10.1016/j.probengmech.2011.08.013.

Ciampoli, M., F. Petrini, and G. Augusti. 2011. "Performance-based wind engineering: Towards a general procedure." *Struct. Saf.* 33 (6): 367–378. https://doi.org/10.1016/j.strusafe.2011.07.001.

Cui, W., and L. Caracoglia. 2015. "Simulation and analysis of intervention costs due to wind-induced damage on tall buildings." *Eng. Struct.* 87 (Mar): 183–197. https://doi.org/10.1016/j.engstruct.2015.01.001.

Cui, W., and L. Caracoglia. 2016. "Exploring hurricane wind speed along US Atlantic coast in warming climate and effects on predictions of structural damage and intervention costs." *Eng. Struct.* 122 (Sep): 209–225. https://doi.org/10.1016/j.engstruct.2016.05.003.

Cui, W., and L. Caracoglia. 2017. "Examination of experimental variability in HFFB testing of a tall building under multi-directional winds." *J. Wind Eng. Ind. Aerodyn.* 171 (Dec): 34–49. https://doi.org/10.1016/j.jweia.2017.09.001.

Cui, W., and L. Caracoglia. 2018a. "A fully-coupled generalized model for multi-directional wind loads on tall buildings: A development of the quasi-steady theory." *J. Fluids Struct.* 78 (Apr): 52–68. https://doi.org/10.1016/j.jfluidstructs.2017.12.008.

Cui, W., and L. Caracoglia. 2018b. "A unified framework for performance-based wind engineering of tall buildings in hurricane-prone regions based on lifetime intervention-cost estimation." *Struct. Saf.* 73 (Jul): 75–86. https://doi.org/10.1016/j.strusafe.2018.02.003.

Cui, W., and L. Caracoglia. 2019. "A new stochastic formulation for synthetic hurricane simulation over the north Atlantic ocean." *Eng. Struct.* 199 (Nov): 109597. https://doi.org/10.1016/j.engstruct.2019.109597.

Davenport, A. G. 1971. "The response of six building shapes to turbulent wind." *Philos. Trans. R. Soc. London, Ser. A* 269 (1199): 385–394. https://doi.org/10.1098/rsta.1971.0039.

Davenport, A. G. 1988. "The response of supertall buildings to wind." In *Second century of the skyscraper*, 705–725. New York: Springer.

Ellingwood, B., D. Rosowsky, Y. Li, and J. Kim. 2004. "Fragility assessment of light-frame wood construction subjected to wind and earthquake hazards." *J. Struct. Eng.* 130 (12): 1921–1930. https://doi.org/10.1061/(ASCE)0733-9445(2004)130:12(1921).

Huang, M., Q. Li, C. Chan, W. Lou, K. C. Kwok, and G. Li. 2015. "Performance-based design optimization of tall concrete framed structures subject to wind excitations." *J. Wind Eng. Ind. Aerodyn.* 139 (Apr): 70–81. https://doi.org/10.1016/j.jweia.2015.01.005.

Hwang, J., Y. Huang, Y. Hung, and J. Huang. 2004. "Applicability of seismic protective systems to structures with vibration-sensitive equipment." *J. Struct. Eng.* 130 (11): 1676–1684. https://doi.org/10.1061/(ASCE)0733-9445(2004)130:11(1676).

Ierimonti, L., L. Caracoglia, and I. Venanzi. 2016. "Probability-based direct numerical estimation of wind-induced non-structural damage on tall buildings." In *Proc., 8th Int. Colloquium on Bluff Body Aerodynamics (BBAA VIII)*. Boston: Northeastern Univ.

Ierimonti, L., L. Caracoglia, I. Venanzi, and A. L. Materazzi. 2017. "Investigation on life-cycle damage cost of wind-excited tall buildings considering directionality effects." *J. Wind Eng. Ind. Aerodyn.* 171 (Dec): 207–218. https://doi.org/10.1016/j.jweia.2017.09.020.

Inokuma, A. 2002. "Basic study of performance-based design in civil engineering." *J. Prof. Issues Eng. Educ. Pract.* 128 (1): 30–35. https://doi.org/10.1061/(ASCE)1052-3928(2002)128:1(30).

Jain, A. 2013. "Wind borne debris impact generated damage to cladding of high-rise building." In *Proc., 12th Americas Conf. on Wind Engineering (12-ACWE)*. Reston, VA: ASCE.

Jain, A. 2015. "Hurricane wind-generated debris impact damage to the glazing of a high-rise building." In *Proc., 7th Congress on Forensic Engineering: Performance of the Built Environment*. Reston, VA: ASCE.

Kwok, K. C., P. A. Hitchcock, and M. D. Burton. 2009. "Perception of vibration and occupant comfort in wind-excited tall buildings." *J. Wind Eng. Ind. Aerodyn.* 97 (7–8): 368–380. https://doi.org/10.1016/j.jweia.2009.05.006.

Lawson, T. 1978. "The wind content of the built environment." *J. Wind Eng. Ind. Aerodyn.* 3 (2–3): 93–105. https://doi.org/10.1016/0167-6105(78)90002-8.

Le, V., and L. Caracoglia. 2018. "Computationally efficient stochastic approach for the fragility analysis of vertical structures subjected to thunderstorm downburst winds." *Eng. Struct.* 165 (Jun): 152–169. https://doi.org/10.1016/j.engstruct.2018.03.007.

Melbourne, W. H. 1980. "Comparison of measurements on the CAARC standard tall building model in simulated model wind flows." *J. Wind Eng. Ind. Aerodyn.* 6 (1): 73–88. https://doi.org/10.1016/0167-6105(80)90023-9.

Moghim, F., and L. Caracoglia. 2012. "A numerical model for wind-borne compact debris trajectory estimation: Part 1—Probabilistic analysis of trajectory in the proximity of tall buildings." *Eng. Struct.* 38 (May): 153–162. https://doi.org/10.1016/j.engstruct.2011.11.020.

Mudd, L., Y. Wang, C. Letchford, and D. Rosowsky. 2014. "Assessing climate change impact on the US east coast hurricane hazard: Temperature, frequency, and track." *Nat. Hazards Rev.* 15 (3): 04014001. https://doi.org/10.1061/(ASCE)NH.1527-6996.0000128.

NOAA (National Oceanic and Atmospheric Administration). 2015. "National data buoy center." Accessed September 30, 2015. http://www.ndbc.noaa.gov/.

Petrini, F., M. Ciampoli, and G. Augusti. 2011. "The role of uncertainties in aeolian risk assessment." In *Computational methods in stochastic dynamics, 187–208*. Dordrecht, Netherlands: Springer.

Rizzo, F., L. Caracoglia, and S. Montelpare. 2018. "Predicting the flutter speed of a pedestrian suspension bridge through examination of laboratory experimental errors." *Eng. Struct.* 172 (Oct): 589–613. https://doi.org/10.1016/j.engstruct.2018.06.042.

SEAOC (Structural Engineers Association of California). 1995. *Vision 2000: Performance based seismic engineering of buildings.* Sacramento, CA: SEAOC.

Seo, D. W., and L. Caracoglia. 2012. "Statistical buffeting response of flexible bridges influenced by errors in aeroelastic loading estimation." *J. Wind Eng. Ind. Aerodyn.* 104–106 (May–Jul): 129–140. https://doi.org/10.1016/j.jweia.2012.03.036.

Seo, D. W., and L. Caracoglia. 2013. "Estimating life-cycle monetary losses due to wind hazards: Fragility analysis of long-span bridges." *Eng. Struct.* 56 (Nov): 1593–1606. https://doi.org/10.1016/j.engstruct.2013.07.031.

Simiu, E., and R. H. Scanlan. 1996. *Wind effects on structures: Fundamentals and applications to design*. 3rd ed. New York: Wiley.

Smith, M. A., and L. Caracoglia. 2011. "A Monte Carlo based method for the dynamic 'fragility analysis' of tall buildings under turbulent wind loading." *Eng. Struct.* 33 (2): 410–420. https://doi.org/10.1016/j.engstruct.2010.10.024.

Spence, S. M., and M. Gioffrè. 2012. "Large scale reliability-based design optimization of wind excited tall buildings." *Probab. Eng. Mech.* 28 (Apr): 206–215. https://doi.org/10.1016/j.probengmech.2011.08.001.

Spence, S. M., and A. Kareem. 2014. "Performance-based design and optimization of uncertain wind-excited dynamic building systems." *Eng. Struct.* 78 (Nov): 133–144. https://doi.org/10.1016/j.engstruct.2014.07.026.

van de Lindt, J., and T. Dao. 2009. "Performance-based wind engineering for wood-frame buildings." *J. Struct. Eng.* 135 (2): 169–177. https://doi.org/10.1061/(ASCE)0733-9445(2009)135:2(169).

Vickery, P. J., F. J. Masters, M. D. Powell, and D. Wadhera. 2009. "Hurricane hazard modeling: The past, present, and future." *J. Wind Eng. Ind. Aerodyn.* 97 (7): 392–405. https://doi.org/10.1016/j.jweia.2009.05.005.

Vickery, P. J., P. Skerlj, and L. Twisdale. 2000. "Simulation of hurricane risk in the US using empirical track model." *J. Struct. Eng.* 126 (10): 1222–1237. https://doi.org/10.1061/(ASCE)0733-9445(2000)126:10(1222).

Vickery, P. J., and L. A. Twisdale. 1995. "Wind-field and filling models for hurricane wind-speed predictions." *J. Struct. Eng.* 121 (11): 1700–1709. https://doi.org/10.1061/(ASCE)0733-9445(1995)121:11(1700).

Wen, Y. K., and Y. J. Kang. 2001. "Minimum building lifecycle cost design criteria. I: Methodology." *J. Struct. Eng.* 127 (3): 330–337. https://doi.org/10.1061/(ASCE)0733-9445(2001)127:3(330).

Xu, Y., T. Liu, and W. Zhang. 2009. "Buffeting-induced fatigue damage assessment of a long suspension bridge." *Int. J. Fatigue* 31 (3): 575–586. https://doi.org/10.1016/j.ijfatigue.2008.03.031.

Xu, Y.-L., and J. He. 2017. *Smart civil structures*. Boca Raton, FL: CRC Press.